Iranian Journal of Astronomy and Astrophysics
Vol. 12, No. 2, Spring 2025, 191–207
©Available online at http://ijaa.du.ac.ir
DOI: 10.22128/ijaa.2025.2994.1218
Online ISSN: 2383–403X

Iranian Journal of Astronomy and Astrophysics

Research Paper

In-Depth Study of the Baryon-Quark Phase Transition in Supernova Matter based on the PNJL Quark Model

Seyyed Alireza Ghaemmaghami[1] · Mehdi Ghazanfari Mojarrad*[2]

[1] Department of Physics, Faculty of Science, University of Kashan, P.O.B 87317-53153, Kashan, Iran;
E-mail: s.ghaemmaghami08@gmail.com

[2] Department of Physics, Faculty of Science, University of Kashan, P.O.B 87317-53153, Kashan, Iran;
*E-mail: ghazanfari@kashanu.ac.ir

Received: 16 July 2025; **Accepted:** 10 December 2025; **Published:** 22 December 2025

Abstract. Determining the equation of state (EOS) of supernova matter is crucial for studying the baryon-quark phase transition (PT) in the inner core of newborn hot neutron stars, thereby deepening the astrophysical investigations on compact objects. For this purpose, we model the baryon-quark PT under the Maxwell construction (MC) by considering a statistical model based on the Thomas-Fermi (TF) approximation for baryonic matter and the Polyakov-Nambu-Jona-Lasino (PNJL) quark model. Furthermore, we adopted interactions MS96 and MS90 for baryonic matter, as well as the vector interaction effects for quark matter. In this work, we focus on the analysis of thermal contributions to the hot hybrid EOS (HHEOS), extracting the thermal index as a basic evaluation parameter. Notably, our study highlights that the HHEOS is strongly affected by the baryonic interaction, neutrino trapping, and especially the quark vector interaction.

Keywords: Statistical Model, PNJL Quark Model, Baryon-Quark Phase Transition, Equation of State.

1 Introduction

The investigation of the phase transition (PT) between baryonic matter and quark matter at finite temperatures represents a significant and influential issue within the domains of particle physics, nuclear physics, and astrophysics, attracting the interest of numerous researchers [1–11]. The baryon-quark PT occurs at extremely high temperatures and densities, which are comparable to the conditions that prevailed in the early stages of the universe following the Big Bang or in heavy ion collisions. In this area, probing the baryon-quark PT under extreme temperatures (50-200 MeV) and densities (5-10 times nuclear saturation density) allows us to mirror the early universe and heavy-ion collisions, thereby expanding the frontiers of our knowledge. The Lattice-QCD provides insights at small baryonic chemical potentials near zero, focusing on the high-temperature (about 150 to 200 MeV), low-baryon-density

* *Corresponding author*

regime [12], while effective models like Nambu-Jona-Lasino (NJL)/Polyakov-Nambu-Jona-Lasino (PNJL) explore high densities and finite baryonic chemical potentials, with transitions at lower temperatures (down to about 50 to 100 MeV) according to the QCD phase diagram. Considering the computational complexity involved in investigating this PT and the behavior of matter in the pure phase, phenomenological models [13–22] can be utilized for effective modeling. The parameters of the phenomenological model are adjusted according to experimental data on nuclear properties at saturation density or the properties of hadronic particles. Ultimately, researchers can obtain thermodynamic quantities at finite temperatures by determining the equation of state (EOS). One of the phenomenological models that effectively describes baryonic matter through the determination of the EOS is the statistical model based on the Thomas-Fermi (TF) approximation [23–31], where the states of particles are characterized by their positions and momenta in phase space. In this model, the thermodynamic properties of baryonic matter can be satisfactorily determined using Myers and Swiatecki (MS) interactions [32–34]. Additionally, several models have been proposed to elucidate the properties of quark matter, such as the NJL [35–44] and PNJL [45–54] phenomenological models, which have been recognized as effective theoretical frameworks. The PNJL model enhances the NJL model by incorporating the Polyakov loop and considering confinement, which makes it a more effective tool for exploring the thermal effects of quark matter and baryon-quark PT. Recent theoretical studies indicate that the QCD phase diagram at high baryon density and low temperature may be considerably richer than a simple hadron–quark dichotomy. In particular, color-superconducting phases (e.g. 2SC and CFL) have been widely discussed as candidate ground states of cold dense matter [55]. Spatially inhomogeneous chiral or density-wave phases have likewise been predicted within NJL-type and related models, which can substantially modify the phase structure [56]. External conditions such as strong magnetic fields and rapid rotation further enrich this picture: magnetic fields tend to favor inhomogeneous condensates (e.g. MDCDW), while rotation can affect the stability and morphology of such phases [57–59]. At the same time, multimessenger observations combined with Bayesian inference techniques have recently provided quantitative constraints on the cold dense-matter equation of state, offering complementary limits to microscopic model studies [60–62]. In the present work we do not include spatial inhomogeneities, magnetic or rotational effects; rather, our two-phase Maxwell construction based on a Thomas–Fermi baryonic description and a PNJL quark model is intended to provide a clear baseline for future studies that incorporate these additional QCD phases and external conditions. For the astrophysical evaluation of the Hot hybrid EOS (HHEOS), we employ in this research a statistical model based on the TF approximation for baryonic matter and the PNJL model for quark matter, allowing the baryon-quark PT to occur under the Maxwell construction (MC), as we have successfully investigated in the previous work [54] the structure and composition of a hot hybrid neutron star based on these phenomenological models. Although the zero-temperature EOSs are appropriate for the structure of neutron stars, certain astrophysical stages are hot and neutrino-rich. Examples are proto-neutron stars shortly after core collapse and the immediate remnants of binary neutron-star mergers, where temperatures can reach tens of MeV and neutrino trapping is possible. To cover these cases we compute HHEOSs (temperature range 20–100 MeV) and compare neutrino-free and neutrino-trapped compositions to quantify how heat and lepton content modify the baryon–quark transition. Consequently, we intend to undertake a astrophysical analysis of the thermal effects on the baryon-quark PT within the framework of this modeling. In accordance with the aforementioned comments, we have structured this manuscript in the following manner: The formalism of the proposed models for determining the EOS based on MC is presented in Sec 2. In Sec. 3, the results obtained from our calculations are analyzed. Finally, the summary and conclusions are delineated in

Sec. 4.

2 Formalism

In the two-phase model, the baryonic phase and the quark phase are depicted using a statistical model based on the TF approximation and the PNJL model, respectively. In studying the baryon-quark PT, the MC is employed, which ensures thermodynamic equilibrium between the phases by requiring equality of pressures and baryonic chemical potentials at the transition point. This construction is derived from the pressures of the baryonic and quark phases as

$$P^{(\mathrm{BP})} = P^{(\mathrm{QP})} = P^{(\mathrm{MP})}, \tag{1}$$

and the baryonic chemical potentials as

$$\mu_B^{(\mathrm{BP})} = \mu_B^{(\mathrm{QP})} = \mu_B^{(\mathrm{MP})}. \tag{2}$$

Here, $P^{(\mathrm{i})}$ and $\mu_B^{(\mathrm{i})}$ (with i = BP, QP, MP) represent the pressures and baryonic chemical potentials in the baryonic phase (BP), quark phase (QP), and mixed phase (MP), respectively.

2.1 Baryonic model

In the initial step of describing the two-phase the HHEOS, we shall adopt MS interaction to model baryonic matter as follows [29,30,54]

$$V_{12} = \frac{-2T_b g\left(\frac{r_{12}}{a}\right)}{\rho_0}\left\{\frac{1}{2}(1\mp\xi)\alpha - \frac{1}{2}(1\mp\zeta)\left[\beta\left(\frac{p_{12}}{p_b}\right)^2 - \gamma\left(\frac{p_b}{|p_{12}|}\right) + \sigma\left(\frac{2\bar{\rho}}{\rho_0}\right)^{\frac{2}{3}}\right]\right\}, \tag{3}$$

with

$$g\left(\frac{r_{12}}{a}\right) = \frac{1}{4\pi a^3}\frac{\exp\left(-\frac{r_{12}}{a}\right)}{\frac{r_{12}}{a}}, \tag{4}$$

$$\bar{\rho}^{\frac{2}{3}} = \frac{1}{2}(\rho_1^{\frac{2}{3}} + \rho_2^{\frac{2}{3}}), \tag{5}$$

where the relative position $r_{12} = |\vec{r}_1 - \vec{r}_2|$ and momentum $p_{12} = |\vec{p}_1 - \vec{p}_2|$ of each nucleonic are defined in phase space. Moreover, r_0, $\rho_0 = (\frac{4}{3}\pi r_0^3)^{-1}$, $\bar{m}$, $p_b = \hbar(\frac{3}{2}\rho_b\pi^2)^{\frac{1}{3}}$, and $T_b = \frac{p_b^2}{2\bar{m}}$ denote the nuclear matter radius, the saturation density, the average nucleonic mass, the Fermi momentum and the associated kinetic energy in this statistical model. In the present work, the baryonic phase is composed solely of nucleons (neutrons and protons) within the statistical model based on the Thomas–Fermi approximation. Hyperons are not included, as the purpose of this study is to focus on the baryon–quark PT in its simplest two-phase form. The adjustable interaction parameters of Eq. (3) within the two sets MS96 (MS90) are ascertained through the fitting of the Weizsacher-Bethe semiempirical mass formula and the saturation properties of nuclear matter, as outlined below [29,32,33]

$$\begin{aligned}
&\alpha = 1.94684(3.60928), \quad \beta = 0.15311(0.37597), \quad \gamma = 1.13672(0.21329),\\
&\sigma = 1.05(1.33677), \quad \xi = 0.27976(0.44003), \quad \zeta = 0.55665(0.59778),\\
&a = 0.59294(0.59542)\,\mathrm{fm}, \quad r_0 = 1.14(1.13)\,\mathrm{fm}.
\end{aligned} \tag{6}$$

In accordance with the statistical model based on the TF approximation, the nucleon density of the bth nucleon is denoted by

$$\rho_b = \frac{2}{h^3}\int d^3p_1 n_b(p_1), \tag{7}$$

with the occupation number $n_b(p)$, where the phase-space single-particle energy $h_b(p)$, and the effective mass B_b can be obtained by minimizing the thermodynamic potential with respect to the occupation number [29]

$$n_b(p) = \frac{1}{1+\exp[(h_b(p)-\mu_b)/T]}, \tag{8}$$

$$h_b(p) = \frac{p^2}{2B_b} + U_b(p) + \bar{m}c^2, \tag{9}$$

$$B_b = \frac{\bar{m}}{1+\frac{2\rho_b}{\rho_0}\beta_l + \frac{2\rho_{b'\neq b}}{\rho_0}\beta_u}, \tag{10}$$

where the single-particle potential $U_b(p)$ which is given by

$$\begin{aligned} U_b(p) = \quad & \left(-\frac{16\pi p_b T_b}{\rho_0 h^3}\right)\left\{\gamma_l\left(\frac{\psi_b(p)}{p}+\phi_b(p)\right)+\gamma_u\left(\frac{\psi_{b'}(p)}{p}+\phi_{b'}(p)\right)\right\} \\ & +\frac{2\,T_b}{\rho_0}\left\{-\alpha_l\rho_b-\alpha_u\rho_{b'}+\beta_l k_b+\beta_u k_{b'}+\frac{4}{3}\,\sigma_l\,\rho_b(\frac{2\,\rho_b}{\rho_0})^{\frac{2}{3}}\right. \\ & \left.+\frac{5}{6}\sigma_u\,\frac{\rho_{b'}}{2}\,(\frac{2\,\rho_b}{\rho_0})^{\frac{2}{3}}+\frac{\sigma_u\rho_{b'}}{2}\left(\frac{2\rho_{b'}}{\rho_0}\right)^{\frac{2}{3}}\right\}, \end{aligned} \tag{11}$$

with

$$\begin{aligned} \psi_{b(b')}(p_1) &= \int_0^{p_1} p_2^2 n_{b(b')}(p_2)\,dp_2, \\ \phi_{b(b')}(p_1) &= \int_{p_1}^{\infty} p_2\, n_{b(b')}(p_2)\,dp_2, \\ k_{b(b')} &= \frac{2}{h^3}\int\left(\frac{p_1}{p_b}\right)^2 n_{b(b')}(p_1)\,d^3p_1, \end{aligned} \tag{12}$$

is derived from the mean-field (MF) potential $V_b(p)$ as follows

$$h_b(p) = \frac{p^2}{2B_b} + U_b(p) + \bar{m}c^2 = \frac{p^2}{2\bar{m}} + V_b(p) + \bar{m}c^2. \tag{13}$$

It is important to mention that the index l denotes the interaction between like nucleon pairs in the above relation, whereas u denotes the interaction between unlike pairs as

$$\alpha_{l,u} = \frac{1}{2}(1\mp\xi)\alpha, \quad \beta_{l,u} = \frac{1}{2}(1\mp\zeta)\beta, \quad \gamma_{l,u} = \frac{1}{2}(1\mp\zeta)\gamma, \quad \sigma_{l,u} = \frac{1}{2}(1\mp\zeta)\sigma. \tag{14}$$

Subsequently, the energy density is calculated via Eq. (3) using the MF potential $V_b(p_1)$, written as

$$V_b(p_1) = \frac{2}{h^3}\int d^3p_2 n_b(p_2)V_{12} = V_b^b(p_1) + V_b^{b'\neq b}(p_1), \tag{15}$$

with

$$V_b^b(p_1) = -\frac{4T_b}{\rho_0 h^3}\int d^3p_2 n_b(p_2)\left[\alpha_l - \beta_l\left(\frac{p_{12}}{p_b}\right)^2 + \gamma_l\frac{p_b}{|p_{12}|} - \sigma_l\left(\frac{2\bar{\rho}}{\rho_0}\right)^{\frac{2}{3}}\right], \tag{16}$$

$$V_b^{b'}(p_1) = -\frac{4T_b}{\rho_0 h^3}\int d^3p_2 n_{b'}(p_2)\left[\alpha_u - \beta_u\left(\frac{p_{12}}{p_b}\right)^2 + \gamma_u\frac{p_b}{|p_{12}|} - \sigma_u\left(\frac{2\bar{\rho}}{\rho_0}\right)^{\frac{2}{3}}\right]. \tag{17}$$

Therefore, the key quantity of energy density e for beta-stable nuclear matter is defined based on the proposed statistical model as follows

$$e = e_{\rm MS} + e_{L} + e_{\gamma}, \tag{18}$$

with the nucleonic energy density $e_{\rm MS}$, the leptonic energy density e_{L}, and the photon energy density e_{γ} characterized based on the standard blackbody relations [30,54,63–66] given by

$$e_{\rm MS} = \sum_{b=n,p}\frac{2}{h^3}\int d^3p_1\left(\frac{p_1^2}{2\bar{m}} + \frac{1}{2}V_b(p_1) + \bar{m}c^2\right)n_b(p_1), \tag{19}$$

$$e_{L} = \sum_{l=e^-,\mu^-,\nu_e^0,\bar{\nu}_\mu^0}\frac{2}{h^3}\int d^3p\, E_p(p)\, n_l(p), \tag{20}$$

$$e_{\gamma} = \frac{\pi^2}{15}\frac{T^4}{(\hbar c)^3}, \tag{21}$$

where

$$n_l(p) = (1 + \exp[\frac{(E_p(p) - \mu_l)}{T}])^{-1}, \tag{22}$$

$$E_p(p) = \sqrt{(pc)^2 + (m_l c^2)^2}, \tag{23}$$

The modeling of baryonic matter under the beta equilibrium conditions for a neutral mixture of particles can be determined as follows

$$\mu_{n^0} - \mu_{p^+} = \mu_{e^-} - \mu_{L_e} = \mu_{\mu^-} - \mu_{L_\mu}, \tag{24}$$

$$\rho_{p^+} = \rho_{e^-} + \rho_{\mu^-}, \tag{25}$$

where it is adopted for neutrino-trapped matter $\mu_{L_e} = \mu_{\nu_e^0}$ ($\mu_{L_\mu} = -\mu_{\bar{\nu}_\mu^0}$), while it is considered for neutrino-free matter $\mu_{L_e} = 0$ ($\mu_{L_\mu} = 0$) [30,54,64,67]. In order to investigate the thermal effects on the internal structure of hot stars, it is posited that the electron and the muon lepton number are defined as

$$Y_{Le} = \frac{\rho_{e^-} + \rho_{\nu_e^0}}{\rho_{B}} = 0.3, \tag{26}$$

$$Y_{L\mu} = \frac{\rho_{\mu^-} - \rho_{\bar{\nu}_\mu^0}}{\rho_{B}} = 0. \tag{27}$$

Finally, the EOS of baryonic matter can be depicted as

$$P = \sum_{i=N,L}(\mu_i\rho_i) - f, \tag{28}$$

where

$$\rho_{_l} = \frac{2}{h^3}\int d^3p_1 n_l(p_1), \tag{29}$$

$$f = e - Ts, \tag{30}$$

and the entropy density s is given based on the entropy density of nucleons $s_{_N}$, leptons $s_{_L}$, and photons s_γ as

$$\begin{aligned} s &= s_{_N} + s_{_L} + s_\gamma \\ &= \sum_{i=N,L} \frac{-2}{h^3}\Big\{\int d^3p_1 \left[n_i(p_1)\ln(n_i(p_1)) + (1-n_i(p_1))\ln(1-n_i(p_1))\right]\Big\} + \frac{4}{3}\frac{e_\gamma}{T}. \end{aligned} \tag{31}$$

2.2 Quark model

The Lagrangian pertaining to the three-flavor PNJL quark model is given by

$$\begin{aligned} \mathcal{L}_{\rm PNJL} = \; & \bar{q}\left(i\gamma_\mu\partial^\mu - m^0\right)q + G_S\sum_{a=0}^{8}\left[\left(\bar{q}\lambda_a q\right)^2 + \left(\bar{q}\gamma_5\lambda_a q\right)^2\right] - K\left\{\det\left[\bar{q}\left(1+\gamma_5\right)q\right]\right. \\ & \left. + \det\left[\bar{q}\left(1-\gamma_5\right)q\right]\right\} - G_V\sum_{a=0}^{8}\left[\left(\bar{q}\gamma_\mu\lambda_a q\right)^2 + \left(\bar{q}\gamma_5\gamma_\mu\lambda_a q\right)^2\right] - \mathcal{U}(\Phi,\bar{\Phi},T), \end{aligned} \tag{32}$$

where the Polyakov-loop effective potential $\mathcal{U}(\Phi,\bar{\Phi},T)$ based on traced Polyakov loop Φ and its conjugate $\bar{\Phi}$ is expressed as

$$\mathcal{U}(\Phi,\bar{\Phi},T) = T^4\left[-\frac{a(T)}{2}\bar{\Phi}\Phi + b(T)\ln[1 - 6\bar{\Phi}\Phi + 4\left(\bar{\Phi}^3 + \Phi^3\right) - 3(\bar{\Phi}\Phi)^2]\right], \tag{33}$$

with $a(T) = a_0 + a_1\left(\frac{T_0}{T}\right) + a_2\left(\frac{T_0}{T}\right)^2$ and $b(T) = b_3\left(\frac{T_0}{T}\right)^3$. In addition, the Gell-Mann matrices λ_a, the quark field q, the current quark mass matrix $m^0 = \mathrm{diag}\left(m^0_{d^-}, m^0_{u^+}, m^0_{s^-}\right)$, the scalar-isoscalar coupling constant G_S, the vector-isoscalar coupling G_V, and the six-point Kobayashi- Maskawa-t'Hooft interaction K are employed in Eq. (32). In this investigation, coefficients $a_{0,1,2} = [3.51, -2.47, 15.2]$ and $b_3 = -1.75$ in the temperature scale $T_0 = 270\,\mathrm{MeV}$ have been adopted based on references [46,54,68–71]. Moreover, the values of $m^0_{u^+} = m^0_{d^-} = 5.5\,\mathrm{MeV}$, $m^0_{s^-} = 140.7\,\mathrm{MeV}$, $G_S = \frac{1.835}{\Lambda^2}$, $K = \frac{12.36}{\Lambda^5}$, and $\Lambda = 602.3\,\mathrm{MeV}$ are taken from reference [36] according to the fitting results. It should be noted that the vector coupling ratio $\eta_{_V} = G_V/G_S$ is considered due to the uncertainty of the quark vector coupling G_V. Consequently, we can determine the PNJL thermodynamic potential density $\Omega_{\rm PNJL}$ as

$$\begin{aligned} \Omega_{\rm PNJL} = \; & -\sum_{q=u,d,s}\frac{3}{\pi^2}\int_0^\Lambda dpp^2E_p^{(M_q)} - \sum_{q=u,d,s}\frac{1}{\pi^2}\int_0^\infty dpp^2\Big[T\ln\left(1 + Z^3 + 3\bar{\Phi}Z^2 + 3\Phi Z\right) \\ & + T\ln\left(1 + Z'^3 + 3\Phi Z'^2 + 3\bar{\Phi}Z'\right)\Big] - 4K\left\langle\bar{q}_u q_u\right\rangle\left\langle\bar{q}_d q_d\right\rangle\left\langle\bar{q}_s q_s\right\rangle + \sum_{q=u,d,s}2G_S\left\langle\bar{q}_q q_q\right\rangle^2 \\ & - \sum_{q=u,d,s}2G_V\langle q_q^\dagger q_q\rangle^2 + \mathcal{U}(\Phi,\bar{\Phi},T), \end{aligned} \tag{34}$$

with the dynamically generated quark mass, M_q, and the quark chemical potential, $\tilde{\mu}_q$, are defined as follows [38,43]

$$M_q = m_q - 4G_S\langle\bar{q}_q q_q\rangle + 2K\langle\bar{q}_{q'}q_{q'}\rangle\langle\bar{q}_{q''}q_{q''}\rangle, \tag{35}$$

$$\tilde{\mu}_q = \mu_q - 4G_V\langle q_q^\dagger q_q\rangle, \tag{36}$$

where $Z = \exp\left[-\left(\frac{E_p^{(M_q)}-\tilde{\mu}_q}{T}\right)\right]$, $Z' = \exp\left[-\left(\frac{E_p^{(M_q)}+\tilde{\mu}_q}{T}\right)\right]$, and $E_p^{(M_q)} = \sqrt{M_q^2+p^2}$. The minimization of $\Omega_{\rm PNJL}$ with respect to the variables M_q and $\tilde{\mu}_q$ leads to the following results

$$\langle\bar{q}_q q_q\rangle = -\frac{3}{\pi^2}\int_0^\Lambda dpp^2\frac{M_q}{E_p^{(M_q)}} + \frac{3}{\pi^2}\int_0^\infty dpp^2\frac{M_q}{E_p^{(M_q)}}\left[F_q+\bar{F}_q\right], \tag{37}$$

$$\langle q_q^\dagger q_q\rangle = \rho_q = \frac{3}{\pi^2}\int_0^\infty dpp^2\left[F_q-\bar{F}_q\right], \tag{38}$$

where

$$F_q = \frac{Z^3+2\bar{\Phi}Z^2+\Phi Z}{1+Z^3+3\bar{\Phi}Z^2+3\Phi Z}, \tag{39}$$

$$\bar{F}_q = \frac{Z'^3+2\Phi Z'^2+\bar{\Phi}Z'}{1+Z'^3+3\Phi Z'^2+3\bar{\Phi}Z'}. \tag{40}$$

In order to determine the values of Φ and $\bar{\Phi}$, it is essential to minimize $\Omega_{\rm PNJL}$ as [54]

$$\begin{aligned} 0 = \quad & T^4\left[-\frac{a(T)}{2}\bar{\Phi}+6\,b(T)\frac{-\bar{\Phi}+2\Phi^2-\Phi\bar{\Phi}^2}{1-6\bar{\Phi}\Phi+4\left(\bar{\Phi}^3+\Phi^3\right)-3(\bar{\Phi}\Phi)^2}\right] \\ & -\frac{3T}{\pi^2}\sum_{q=u,d,s}\int_0^\infty dpp^2\left[\frac{Z}{1+Z^3+3\bar{\Phi}Z^2+3\Phi Z}+\frac{Z'^2}{1+Z'^3+3\Phi Z'^2+3\bar{\Phi}Z'}\right], \end{aligned} \tag{41}$$

$$\begin{aligned} 0 = \quad & T^4\left[-\frac{a(T)}{2}\Phi+6\,b(T)\frac{-\Phi+2\bar{\Phi}^2-\bar{\Phi}\Phi^2}{1-6\bar{\Phi}\Phi+4\left(\bar{\Phi}^3+\Phi^3\right)-3(\bar{\Phi}\Phi)^2}\right] \\ & -\frac{3T}{\pi^2}\sum_{q=u,d,s}\int_0^\infty dpp^2\left[\frac{Z'^2}{1+Z^3+3\bar{\Phi}Z^2+3\Phi Z}+\frac{Z}{1+Z'^3+3\Phi Z'^2+3\bar{\Phi}Z'}\right]. \end{aligned} \tag{42}$$

The beta equilibrium conditions for a neutral mixture of quarks and leptons can be written as follows

$$\mu_{_B} = \frac{2\mu_{d^-}+\mu_{u^+}}{3} \equiv \frac{\mu_{n^0}}{3}, \tag{43}$$

$$\mu_{u^+} = \mu_{_B} - \frac{2}{3}\left(\mu_{e^-}-\mu_{_{Le}}\right), \tag{44}$$

$$\mu_{d^-} = \mu_{s^-} = \mu_{_B} + \frac{1}{3}(\mu_{e^-}-\mu_{_{Le}}), \tag{45}$$

$$\mu_{e^-}-\mu_{_{Le}} = \mu_{\mu^-}-\mu_{_{L\mu}}, \tag{46}$$

with $Y_{Le} = 0.3$ for neutrino-trapped matter and $\mu_{_{Le}} = 0$ for neutrino-free matter. The charge neutrality condition can also be considered as

$$\frac{2}{3}\rho_{u^+} - \frac{1}{3}\left(\rho_{d^-}+\rho_{s^-}\right) - \left(\rho_{e^-}+\rho_{\mu^-}\right) = 0. \tag{47}$$

By taking $\Omega^0_{\rm PNJL}$ as the thermodynamic potential in the vacuum (evaluated at $T_0 = \mu_q = 0$, and $\Phi = \bar{\Phi} = 0$), the vacuum (Dirac sea) contribution is subtracted from the PNJL thermodynamic potential density $\Omega_{\rm PNJL}$ to guarantee that the pressure of quark matter vanishes in the vacuum. Although the divergent integrals are regularized by the sharp

cutoff, this subtraction ensures the proper normalization of the thermodynamic potential and removes the constant vacuum energy [38]. Hence, the EOS of quark matter can be obtained as follows

$$P = P_{\mathrm{PNJL}} + P_{_L} + P_{\gamma}, \tag{48}$$

where

$$P_{\mathrm{PNJL}} = \Omega^{0}_{\mathrm{PNJL}} - \Omega_{\mathrm{PNJL}}, \tag{49}$$

$$P_{_L} = \sum_{l=e^-,\mu^-,\nu_e^0,\bar{\nu}_\mu^0} (\mu_l \rho_l) - e_{_L} + T s_{_L}, \tag{50}$$

$$P_{\gamma} = \frac{e_{\gamma}}{3}. \tag{51}$$

Therefore, the different quantities of free energy density f, entropy density s, and energy density e are given by

$$f = \sum_{k=Q,L} (\mu_k \rho_k) - P, \tag{52}$$

$$s = -\frac{\partial \Omega_{\mathrm{PNJL}}}{\partial T}, \tag{53}$$

$$e = Ts + f. \tag{54}$$

3 Results and discussions

The constituent quark masses M_q for up (M_u), down (M_d), and strange (M_s) quarks as a function of the baryonic chemical potential μ_B in Figure 1. The masses remain nearly constant at low μ_B before decreasing sharply, indicating the onset of chiral symmetry restoration. The inclusion of vector interaction ($\eta_V = 0.3$) results in slightly higher masses at lower μ_B, due to the repulsive nature of the vector channel, which stiffens the quark matter EOS and delays the mass reduction. In addition, neutrino trapping shifts the curves towards higher masses. Multiple curves in each panel correspond to increasing temperatures (e.g., $T = 20, 40, 60, 80, 100$ MeV), where higher T leads to a more pronounced and earlier mass reduction, reflecting enhanced thermal effects driving the system toward restoration.

The Polyakov loop values Φ and $\bar{\Phi}$ as a function of the baryonic chemical potential μ_B in Figure 2. The Polyakov loops increase with μ_B, indicating deconfinement, with notable shifts due to neutrino trapping and vector repulsion effects. The loops start at low μ_B (confined phase) and rise toward higher values, signaling deconfinement. Furthemore, vector interactions introduce a slight suppression in the loop values. Our result indicated that with rising temperature, the Polyakov loops increase more rapidly. Neutrino trapping does not have a significant effect on the values of Φ and $\bar{\Phi}$. As can be seen, the value of $\bar{\Phi}$ is greater than Φ in all cases examined.

For a better understanding of the thermal effects, one can survey the thermal pressure P_{th} and thermal energy density e_{th}, which can be calculated as follows

$$P_{\mathrm{th}}\left(T, \rho_B\right) = P\left(T, \rho_B\right) - P\left(T = 0, \rho_B\right), \tag{55}$$

$$e_{\mathrm{th}}\left(T, \rho_B\right) = e\left(T, \rho_B\right) - e\left(T = 0, \rho_B\right), \tag{56}$$

where the total pressure P and energy density e at each baryonic density are obtained under the MC. In the pure baryonic phase, the total pressure (energy density) is given according

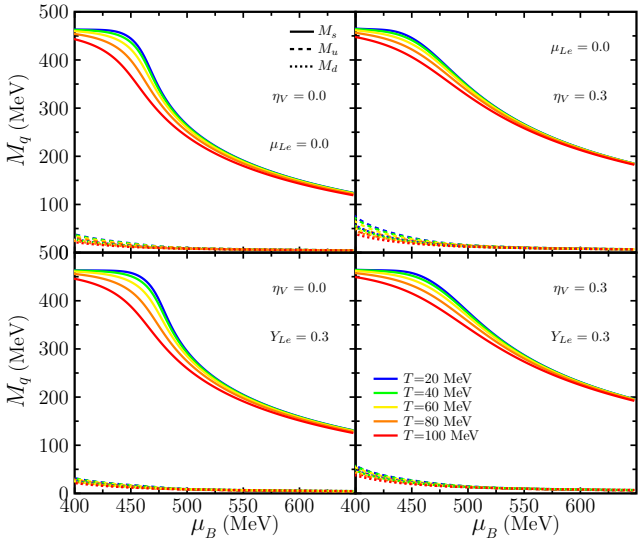

Figure 1: Constituent quark masses as a function of baryonic chemical potential in neutrino-free matter (top panels) and neutrino-trapped matter (bottom panels) at temperatures $T = 20, 40, 60,$ 80, and 100 MeV with the vector strength ratios $\eta_V = 0$ (left panels) and $\eta_V = 0.3$ (right panels).

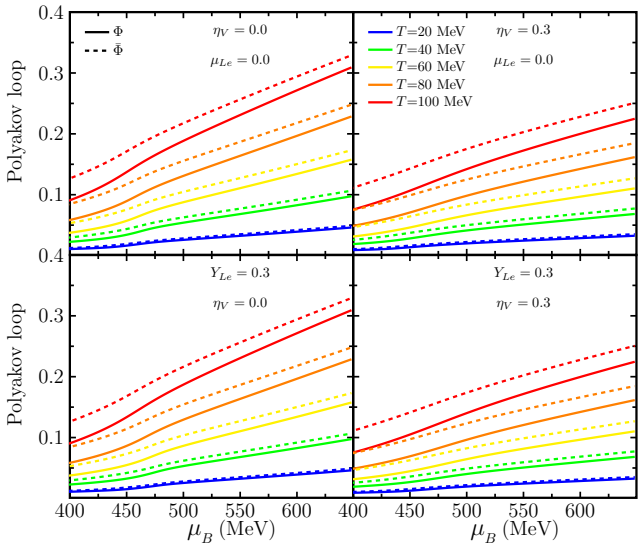

Figure 2: Polyakov loop values Φ and $\bar{\Phi}$ as a function of baryonic chemical potential in neutrino-free matter (top panels) and neutrino-trapped matter (bottom panels) at temperatures $T = 20, 40, 60,$ 80, and 100 MeV with the vector strength ratios $\eta_V = 0$ (left panels) and $\eta_V = 0.3$ (right panels).

to Eq. (28) (Eq. (18)), whereas in the pure quark phase, the total pressure (energy density) refers to Eq. (48) (Eq.(54)).

Figures 3 and 4 demonstrate the $P_{\rm th}$ as a function of baryonic density ρ_B for neutrino-

free matter and neutrino-trapped matter, respectively. When the MP occurs at least in one of $P(T, \rho_B)$ or $P(T = 0, \rho_B)$ in Eq. (55), one can define the extended mixed phase (EMP) zone identified by the dashed lines in these figures. As also shown, the EMP region can be linearly interpolated to avoid the jumps of $P_{\rm th}$ during the first-order phase transition. As a result, $P_{\rm th}$ experiences a significant drop from the beginning to the end of the EMP domain. Given that $P_{\rm th}$ is an increasing function of ρ_B in the pure baryonic region, this quantity for MS96 reaches higher values than that of MS90. In the pure quark region, neutrino-free matter has a decreasing behavior with the baryonic density, while neutrino-trapped matter reaches a smooth increasing function. The findings demonstrate that the values of $P_{\rm th}$ increase with temperature. According to observations, the density range of the EMP region typically increases in response to rising temperatures. In general, vector interactions are observed to push the points of the EMP toward increased values of $P_{\rm th}$ and ρ_B.

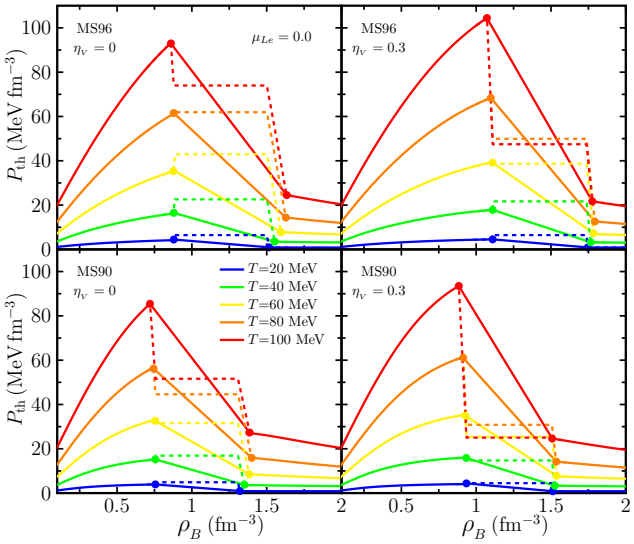

Figure 3: Thermal pressure as a function of baryonic density for the hybrid phase of neutrino-free matter at temperatures $T = 20, 40, 60, 80$, and $100\,$MeV, using the baryonic interactions MS96 (top panels) and MS90 (bottom panels), and the PNJL quark model with the vector strength ratios $\eta_V = 0$ (left panels) and $\eta_V = 0.3$ (right panels) within the MC. The EMP regions are pinpointed by the pairs of the solid dots.

The thermal energy density $e_{\rm th}$ vs. baryonic density ρ_B is demonstrated for neutrino-free matter and neutrino-trapped matter in Figures 5 and 6, respectively. At first glance, it is clearly recognized that the EMP region significantly reflects the thermal effects. As a general trend, $e_{\rm th}$ increases with ρ_B, given that the temperature intensifies this upward trend, especially for the EMP region. As a result of rising temperature, $e_{\rm th}$ is always pushed toward higher values. Furthermore, within the range of the baryonic density, a decrease in the width of pure quark matter is observed as an outcome of neutrino trapping. It is evident that MS96 increases the energy density range of the EMP compared to MS90, pushing it towards higher values.

To examine the thermal effects more precisely, we show in Figures 7 and 8, the ratios $\frac{P_{\rm th}}{P_0}$ and $\frac{e_{\rm th}}{e_0}$ ($P_0 = P(T = 0, \rho_B)$ and $e_0 = e(T = 0, \rho_B)$ are the cold pressure and energy density) at the intended baryonic density range, respectively. According to these figures, The values of $\frac{P_{\rm th}}{P_0}$ ($\frac{e_{\rm th}}{e_0}$) at each ρ_B become closer to each other, as the temperature rises.

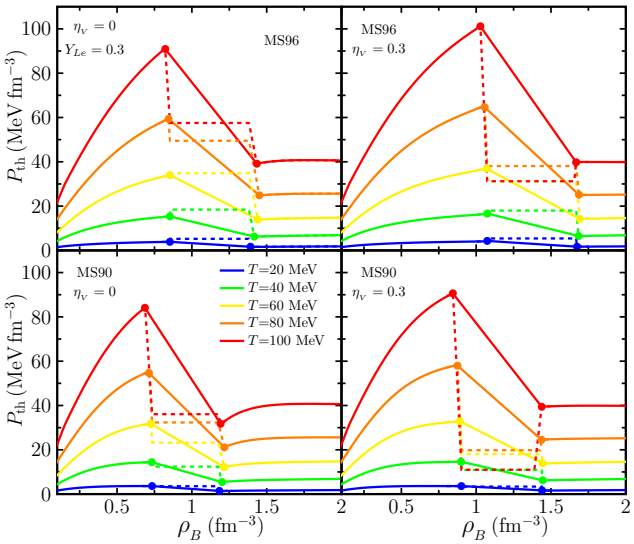

Figure 4: Same as Figure (3) but for the hybrid phase of neutrino-trapped matter.

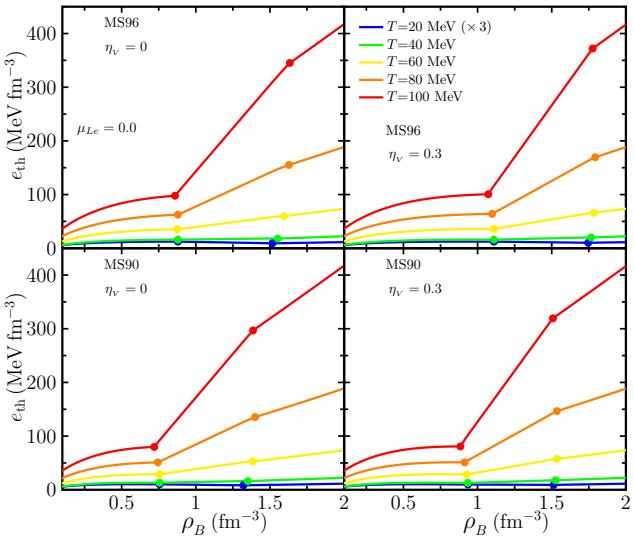

Figure 5: Thermal energy density as a function of baryonic density for the hybrid phase of neutrino-free matter at temperatures $T = 20$ (multiplied by three), 40, 60, 80, and 100 MeV, using the baryonic interactions MS96 (top panels) and MS90 (bottom panels), and the PNJL quark model with the vector strength ratios $\eta_V = 0$ (left panels) and $\eta_V = 0.3$ (right panels) according to the MC. The EMP regions are pinpointed by the pairs of the solid dots.

Thus, the thermal effects become more pronounced at lower temperatures. In general, the ratio $\frac{P_{\rm th}}{P_0}$ has a decreasing trend with increasing density. On the contrary, the ratio $\frac{e_{\rm th}}{e_0}$ is mainly identified by a non-monotonic behavior. It can be observed that increasing η_V leads the baryon-quark EMP to occur at lower values of these ratios. Moreover, $\frac{P_{\rm th}}{P_0}$ and $\frac{e_{\rm th}}{e_0}$ become mostly larger as a result of neutrino trapping. Nevertheless, changing the

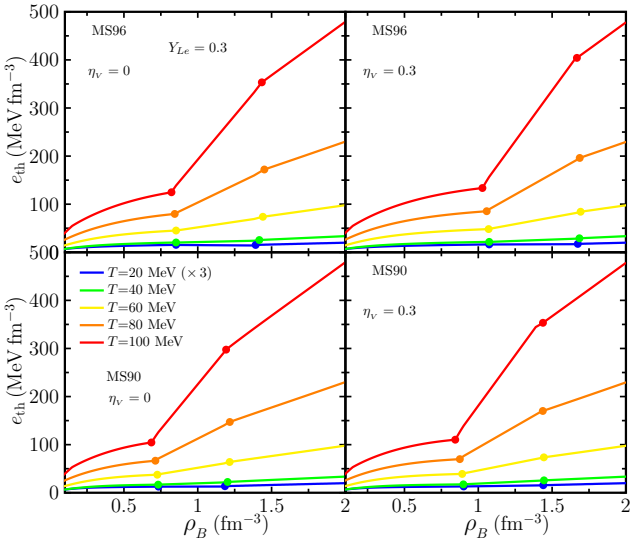

Figure 6: Same as Figure (5) but for the hybrid phase of neutrino-trapped matter.

baryonic interaction from MS96 to MS90 does not have a considerable consequence for these quantities.

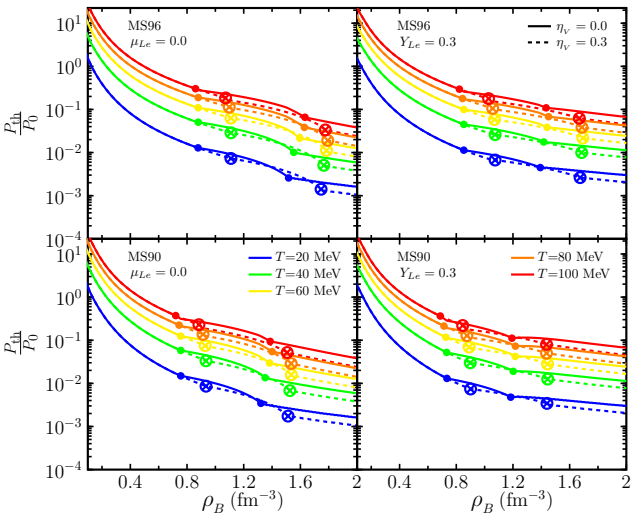

Figure 7: Ratio of thermal Pressure to cold matter pressure as a function of baryonic density for the hybrid phases of neutrino-free matter (left panels) and neutrino-trapped matter (right panels) at temperatures $T = 20, 40, 60,$ 80, and 100 MeV, using the baryonic interactions MS96 (top panels) and MS90 (bottom panels), as well as the PNJL quark model with the vector strength ratios $\eta_V = 0$ (solid lines) and $\eta_V = 0.3$ (dashed lines) based on the MC. The EMP regions are symbolized by the pairs of the solid dots (circled times) for $\eta_V = 0$ ($\eta_V = 0.3$).

By adopting the Γ-law approximation, the thermal index $\Gamma_{\rm th} = 1 + \frac{P_{\rm th}}{e_{\rm th}}$ is regarded as

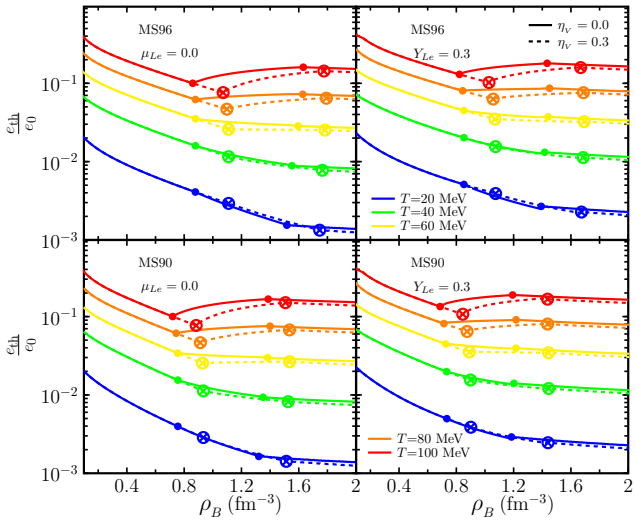

Figure 8: Ratio of thermal energy density to cold matter energy density as a function of baryonic density for the hybrid phases of neutrino-free matter (left panels) and neutrino-trapped matter (right panels) at temperatures $T = 20, 40, 60,$ 80, and 100 MeV, using the baryonic interactions MS96 (top panels) and MS90 (bottom panels), accompanied by the PNJL quark model with the vector strength ratios $\eta_V = 0$ (solid lines) and $\eta_V = 0.3$ (dashed lines) based on the MC. The EMP regions are signified by the pairs of the solid dots (circled times) for $\eta_V = 0$ ($\eta_V = 0.3$).

an important parameter, by which the EOS of dense matter at each temperature, especially in astrophysical simulations, can be evaluated. Hence, the temperature and baryonic dependence of $\Gamma_{\rm th}$ is demonstrated in Figure 9. As can be seen, the sensitivity of $\Gamma_{\rm th}$ to the baryonic density is more significant in neutrino-free matter than in neutrino-trapped matter. When the temperature increases, a decrease in this parameter is indicated. Our calculations imply that $\Gamma_{\rm th}$ in the pure quark region lies just below the conventional astrophysical range $1.5 < \Gamma_{\rm th} < 2$ [72–74]. It should be noted that the larger $\Gamma_{\rm th}$ values belong to the hybrid EOSs using MS90 than those obtained by MS96. In addition, the temperature and quark vector interaction appreciably change the amount of $\Gamma_{\rm th}$ in the EMP region.

4 Summary and conclusion

This study aims to enhance our understanding of thermal effects in an astrophysical context by introducing the HHEOSs related to the baryon-quark PT under MC. In particular, we investigated two scenarios involving neutrino-free and neutrino-trapped matter. For this purpose, we described the EOS of baryonic matter using the MF model based on the TF approximation and taking into account the baryonic interactions MS96 and MS90. To comprehend the thermal properties of quark matter, the PNJL model is utilized to conduct a comprehensive study, with an emphasis on the vector interactions that occur between quarks. It has been observed that the density range of the EMP region typically expands in response to rising temperatures. According to the findings, the thermal index (which is a parameter characterizing the thermal effects in the astrophysical simulations) decreases as temperature increases, while the thermal pressure, thermal energy density, and their

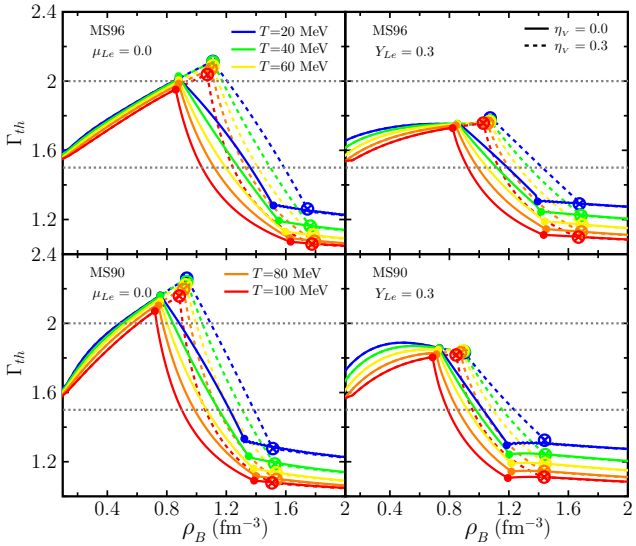

Figure 9: Thermal index as a function of baryonic density for the hybrid phases of neutrino-free matter (left panels) and neutrino-trapped matter (right panels) at temperatures $T = 20, 40, 60, 80$, and $100\,\mathrm{MeV}$, utilizing the baryonic interactions MS96 (top panels) and MS90 (bottom panels), as well as the PNJL quark model with the vector strength ratios $\eta_V = 0$ (solid lines) and $\eta_V = 0.3$ (dashed lines) in the framework of the MC. The EMP regions are symbolized by the pairs of the solid dots (circled times) for $\eta_V = 0$ ($\eta_V = 0.3$).

ratios to cold pressure and energy density increase. The calculations performed for the thermal index demonstrate that the temperature and quark vector coupling strongly affect this astrophysical index in the EMP region rather than in the pure baryonic and quark areas. In addition, our study demonstrates that the HHEOS is significantly affected by the type of baryonic interaction, neutrino trapping, and quark vector interaction. This investigation could pave the way for extensive research into the internal structure of hot hybrid neutron stars, potentially uncovering new insights into their composition and behavior under extreme conditions.

Acknowledgment

Authors would like to thank University of Kashan for supporting this project under the grant number 1391802/1 provided by the Research Council.

Authors' Contributions

All authors have the same contribution.

Data Availability

No data available.

Conflicts of Interest

The authors declare that there is no conflict of interest.

Ethical Considerations

The authors have diligently addressed ethical concerns, such as informed consent, plagiarism, data fabrication, misconduct, falsification, double publication, redundancy, submission, and other related matters.

Funding

This research did not receive any grant from funding agencies in the public, commercial, or nonprofit sectors.

References

[1] Menezes, D. P., & Providência, C. 2004, Phys. Rev. C, 69, 045801.

[2] Nicotra, O. E., Baldo, M., Burgio, G. F., & Schulze, H. J. 2006, Phys. Rev. D, 74, 123001.

[3] Burgio, G. F., & Plumari, S. 2008, Phys. Rev. D, 77, 085022.

[4] Yasutake, N., Maruyama, T., & Tatsumi, T. 2009, Phys. Rev. D, 80, 123009.

[5] Bombaci, I., Logoteta, D., Providência, C., & Vidana, I. 2011, Astron. Astrophys., 528, A71.

[6] Chen, H., Baldo, M., Burgio, G. F., & Schulze, H.-J. 2012, Phys. Rev. D, 86, 045006.

[7] Hempel, M., et al. 2016, Phys. Rev. D, 94, 103001.

[8] Mariani, M., Orsaria, M., & Vucetich, H. 2017, Astron. Astrophys., 601, A21.

[9] Fischera, T. 2021, Eur. Phys. J. A, 57, 270.

[10] Logoteta, D., Bombaci, I., & Perego, A. 2022, Eur. Phys. J. A, 58, 55.

[11] Ivanytskyi, O., & Blaschke, D. 2022, Eur. Phys. J. A, 58, 152.

[12] Bazavov, A., et al. 2014, Phys. Rev. D, 90, 094503.

[13] Seyler, R. G., & Blanchard, C. H. 1961, Phys. Rev., 124, 227.

[14] Seyler, R. G., & Blanchard, C. H. 1963, Phys. Rev., 131, 355.

[15] Bandyopadhyay, D., & Samaddar, S. K. 1988, Nucl. Phys. A, 484, 315.

[16] Bandyopadhyay, D., Samanta, C., Samaddar, S. K., & De, J. N. 1990, Nucl. Phys. A, 511, 1.

[17] Chabanat, E., et al. 1998, Nucl. Phys. A, 635, 231.

[18] Strobel, K., Weber, F., & Weigel, M. K. 1999, Z. Naturf. A, 54, 83.

[19] Basu, D. N. 2004, J. Phys. G, 30, B7.

[20] Xu, J., Chen, L. W., Li, B. A., & Ma, H. R. 2007, Phys. Rev. C, 75, 014607.

[21] Moustakidis, C. C. 2008, Phys. Rev. C, 78, 054323.

[22] Moshfegh, H. R., & Ghazanfari Mojarrad, M. 2011, J. Phys. G, 38, 085102.

[23] Moshfegh, H. R., & Ghazanfari Mojarrad, M. 2011, J. Phys. G Nucl. Part. Phys., 38, 085102.

[24] Moshfegh, H. R., & Ghazanfari Mojarrad, M. 2013, Eur. Phys. J. A, 49, 1.

[25] Ghazanfari Mojarrad, M., & Arabsaeidi, R. 2016, Int. J. Mod. Phys. E, 25, 1650102.

[26] Ghazanfari Mojarrad, M., & Mousavi Khoroshtomi, S. K. 2017, Int. J. Mod. Phys. E, 26, 1750038.

[27] Ghazanfari Mojarrad, M., Razavi, N. S., & Vaezzade, S. 2018, Nucl. Phys. A, 980, 51.

[28] Ghazanfari Mojarrad, M., & Razavi, N. S. 2019, Nucl. Phys. A, 986, 133.

[29] Ghaemmaghami, S. A., & Ghazanfari Mojarrad, M. 2022, Eur. Phys. J. A, 58, 255.

[30] Razavi, N. S., & Ghazanfari Mojarrad, M. 2023, Nucl. Phys. A, 1029, 122556.

[31] Ghaemmaghami, S. A., & Ghazanfari Mojarrad, M. 2024, Radiation Physics and Engineering,

[32] Myers, W. D., & Swiatecki, W. J. 1990, Ann. Phys. (N. Y.), 204, 401.

[33] Myers, W. D., & Swiatecki, W. J. 1996, Nucl. Phys. A, 601, 141.

[34] Myers, W. D., & Swiatecki, W. J. 1998, Phys. Rev. C, 57, 3020.

[35] Lutz, M., Klimt, S., & Weise, W. 1992, Nucl. Phys. A, 542, 521.

[36] Rehberg, P., Klevansky, S. P., & Hüfner, J. 1996, Phys. Rev. C, 53, 410.

[37] Hatsuda, T., & Kunihiro, T. 1994, Phys. Rep., 247, 221.

[38] Buballa, M. 2005, Phys. Rep., 407, 205.

[39] Ghazanfari Mojarrad, M., & Ranjbar, J. 2019, Phys. Rev. C, 100, 015804.

[40] Ghazanfari Mojarrad, M., & Ranjbar, J. 2020, Ann. Phys. (N. Y)., 412, 168048.

[41] Liu, H., Xu, J., & Ko, C. M. 2020, Phys. Lett. B, 803, 135343.

[42] Liu, L. M., Zhou, W. H., Xu, J., & Peng, G. X. 2021, Phys. Lett. B, 822, 136694.

[43] Ranjbar, J., & Ghazanfari Mojarrad, M. 2021, Phys. Rev. C, 104, 045807.

[44] Ghaemmaghami, S. A., Khoshi, M. R., & Ghazanfari Mojarrad, M. 2023, Eur. Phys. J. Plus, 138, 1.

[45] Rossner, S., Ratti, C., & Weise, W. 2007, Phys. Rev. D, 75, 034007.

[46] Moreira, J., Hiller, B., Osipov, A. A., & Blin, A. H. 2012, Int. J. Mod. Phys. A, 27, 1250060.

[47] Cui, Z. F., et al. 2014, Eur. Phys. J. C, 74, 1.

[48] Shao, G. Y., et al. 2016, Phys. Rev. D, 94, 014008.

[49] Fuseau, D., Steinert, T., & Aichelin, J. 2020, Phys. Rev. C, 101, 065203.

[50] Wang, Y., & Wen, X. J. 2022, Phys. Rev. D, 105, 074034.

[51] He, W. B., et al. 2022, Phys. Rev. D, 105, 094024.

[52] Maslov, K., & Blaschke, D. 2023, Phys. Rev. D, 107, 094010.

[53] Liu, H., et al. 2024, Phys. Rev. D, 109, 074037.

[54] Ghaemmaghami, S. A., & Ghazanfari Mojarrad, M. 2025, Phys. Rev. D, 111, 023026.

[55] Gholami, H., et al. 2025, Phys. Rev. D, 111, 103034.

[56] Nakano, E., & Tatsumi, T. 2005, Phys. Rev. D, 71, 114006.

[57] Frolov, I. E., Zhukovsky, V. C., & Klimenko, K. G. 2010, Phys. Rev. D, 82, 076002.

[58] Gyory, W., & de la Incera, V. 2022, Physical Review D, 106, 016011.

[59] Tabatabaee Mehr, S. M. A. 2023, Phys. Rev. D, 108, 094042.

[60] Dietrich, T., et al. 2020, Sci., 370, 1450.

[61] Raaijmakers, G., et al. 2021, Astrophys. J. Lett., 918, L29.

[62] Roy, D. G., et al. 2024, Phys. Lett. B, 859, 139128.

[63] Lattimer, J. M., & Swesty, F. D. 1991, Nucl. Phys. A, 535, 331.

[64] Ghaemmaghami, S. A., & Ghazanfari Mojarrad, M. 2023, Eur. Phys. J. Plus, 138, 1.

[65] Constantinou, C., Muccioli, B., Prakash, M., & Lattimer, J. M. 2014, Phys. Rev. C, 89, 065802.

[66] Constantinou, C., Muccioli, B., Prakash, M., & Lattimer, J. M. 2015, Phys. Rev. C, 92, 025801.

[67] Takatsuka, T., Nishizaki, S., & Hiura, J. 1994, Prog. Theor. Phys., 92, 779.

[68] Costa, P., et al. 2009, Phys. Rev. D, 79, 116003.

[69] Bratovic, N., Hatsuda, T., & Weise, W. 2013, Phys. Lett. B, 719, 131.

[70] Hansen, H., Stiele, R., & Costa, P. 2020, Phys. Rev. D, 101, 094001.

[71] Costa, P., Pereira, R. C., & Providência, C. 2020, Phys. Rev. D, 102, 054010.

[72] Bauswein, A., Janka, H. T., & Oechslin, R. 2010, Phys. Rev. D, 82, 084043.

[73] Endrizzi, A., et al. 2018, Phys. Rev. D, 98, 043015.

[74] Torres-Rivas, A., Chatziioannou, K., Bauswein, A., & Clark, J. A. 2019, Phys. Rev. D, 99, 044014.